scientific reports

Check for updates

OPEN

Selective Lis1 inactivation disrupts migration and positioning of cortical somatostatin interneurons

A. Pombero[1,4], R. García-López[1,4]✉, E. Geijo-Barrientos[1] & S. Martínez[1,2,3]✉

One subtype of interneurons, classified by their neurochemical properties, are somatostatin-positive (SST+) interneurons, which express somatostatin along with GABA and form synapses with both pyramidal neurons and other interneurons. SST+ interneurons originate in the medial ganglionic eminence and migrate tangentially to the cortex, making them potentially vulnerable to gene mutations linked to neuronal migration disorders. The *Lis1* gene (Pafah1b1) regulates dynein-mediated motility, mitosis, and microtubule organization. Mutations in *Lis1* are associated with lissencephaly and cortical disorganization. To investigate its role, we developed a mouse model with *Lis1* deletion specifically in SST+ interneurons. We studied the anatomical and developmental effects of this deletion, focusing on tangential migration during embryonic and early postnatal stages. We analyzed SST+ interneuron numbers in the cingulate cortex (anterior and retrosplenial regions) of young mutant mice (P30). Our findings show a reduction in SST+ interneurons in mutants compared to controls, indicating impaired migration and/or maturation. Further research is needed to uncover the mechanisms behind this reduction and to determine its functional implications.

Keywords Lis1, Somatostatin, Cingulate cortex

The mutation in the platelet-activating factor acetyl hydrolase IB subunit alpha (Pafah1b1; also known as Lissecephaly-1 or *Lis1*) is directly linked to lissencephaly type I [1]. Lissencephaly ("smooth brain") presents as a severe condition with highly disabling symptoms such as mental retardation, epilepsy or premature death, characterized primarily by the absence of cortical folds. LIS1 protein is involved in several basic cellular functions such as mitosis, nuclear position, microtubule regulation and neuronal migration, achieved through its interactions with a different array of proteins[2]. Analysis of heterozygous brains carrying the null allele (Lis1+/-) revealed significant observations, notably delays in neuronal migration, cortical and hippocampal disorganization, as well as deficits in spatial learning and epilepsy[3–8]. Another approach to investigate the effects of *Lis1* mutation involved the generation of a mutant allele (*sLis1*) that yields a truncated LIS1 protein incapable of dimerization[9,10]. *sLis/Lis1* mutant mice exhibit delays in the cortical plate formation and in the thalamocortical axons development, along with alterations in the septohippocampal projection development, slower migration, aberrant neuronal morphology and reduced interneuron numbers in anterior cingulate area, and a disbalance in cellular activation, as evidenced by c-fos expression[9–12].

Cortical GABAergic interneurons are essential for the establishment of balanced neocortical circuits and originate predominantly from the ventral telencephalic ganglionic eminences during embryonic development[13–15]. Among these populations, somatostatin-expressing (SST+) interneurons arise mainly from the medial ganglionic eminence (MGE) in a tightly regulated temporal sequence[16,17]. This birthdate dictates their final laminar position and subtype identity: while early-born SST+ cohorts (generated around E12.5-E13.5 in the mouse) primarily populate the deep cortical layers (V–VI), late-born cohorts (generated around E15.5-E16.5) are destined for superficial layers (II–III) and preferentially acquire a Calb2 + Martinotti cell identity[16,18,19]. To reach their cortical destinations, SST+ interneurons migrate tangentially via two main streams: a deep route within the subventricular/intermediate zones (SVZ/IZ) and a superficial route along the marginal zone (MZ)[20]. Crucially, the choice of migratory stream is linked to cellular fate; specifically, migration through the MZ acts as a critical corridor for the dispersion and specification of the late-born, prospective Martinotti population[19,21]. Finally, these cells switch to radial migration to settle in the cortical plate. Disruption of these migratory mechanisms compromises interneuron positioning and survival, ultimately impairing cortical circuit assembly

[1]Instituto de Neurociencias, UMH-CSIC, Campus de San Juan, E- 03550- Alicante, Alicante E-03550, Spain. [2]Centro de Investigación Biomédica En Red en Salud Mental (CIBERSAM), Madrid, Spain. [3]Instituto de Investigación Sanitaria y Biomédica de Alicante (ISABIAL), Alicante, Spain. [4] Pombero A and García-López R. contributed equally to this work. ✉email: ; smartinez@umh.es

and function[22]. In contrast to MGE-derived populations, the Caudal Ganglionic Eminence (CGE) generates a distinct cohort of interneurons, primarily VIP + and Reelin+ subtypes, which migrate later and preferentially populate the superficial cortical layers[23].

Somatostatin-expressing (SST+) interneurons represent a subtype of interneuron based on neurochemical classification[24,25]. SST+ interneurons mainly target the dendrites of pyramidal cells, modulating brain excitability throughout presynaptic mechanisms[26,27]. Notably, somatostatin systems play a crucial role in regulating sensory and cognitive functions, with a decrease in somatostatin expression linked to several neurodegenerative diseases such as Alzheimer's and Parkinson's diseases[28]. In neurological disorders, the cingulate cortex appears particularly vulnerable to the specific loss of SST+ interneurons, leading to dysfunctions of GABAergic signaling[29–31]. The cingulate cortex, situated around the corpus callosum, encompasses a cortical strip that can be further subdivided into various structurally and functionally distinct regions[32,33]. In rodents, the retrosplenial cortex (RSC) encompasses the entire posterior cingulate cortex (areas 29 and 30) whereas the anterior cingulate cortex (ACC) is considered as a part of the medial prefrontal cortex (mPFC), which also includes the infralimbic and prelimbic areas[34,35]. The cingulate cortex plays a crucial role in sensory processing, emotion, reward-related processing, memory tasks, navigation, and prospective thinking. [36–38]. The cingulate region shows a well-documented vulnerability to disruptions in GABAergic signaling, including consistent reductions in somatostatin (SST) expression and SST+ interneuron markers in neuropsychiatric conditions[29–31,39,40]. Given this selective sensitivity, alterations in SST levels are expected to exert a pronounced functional impact in ACC and the closely interconnected RSC. In this study, we investigated the impact of *Lis1* mutation on SST+ interneurons in the mouse cingulate cortex. To achieve this, we developed an animal model where the *Lis1* gene is specifically deleted in SST+ interneurons, allowing us to analyze the role of *Lis1* in long-range migratory interneurons. Our focus was on examining the anatomical and developmental effects of *Lis1* silencing during SST+ interneuron development. Our findings revealed a significant reduction in the number of SST+ interneurons in the cingulate cortex of mutant mice compared to controls during young adulthood. Furthermore, our investigation into the involvement of *Lis1* in SST+ interneurons during cortical development unveiled a severe impairment in this process when *Lis1* is mutated. Based on our observations, *Lis1* appears to play a crucial role in the development of SST+ interneurons.

Results

We have analyzed the organization and prenatal development of the SST+ neurons in the cingulate cortex after the inactivation of the *Lis1* gene in these neurons.

Since the expression of the gene encoding for SST is high in developing cortical interneurons beginning at both E13.5 and E15.5 [41] we first confirmed that Cre activity in SST-Cre driver animals is specific to the SST population using double immunostaining against SST and the red fluorescent protein (RFP) in *Lis1*-SST-RFP animals (Fig. 1). At postnatal day 1 (P1), we observed immunopositivity for both SST and RFP in the anterior cingulate cortex (ACC) and retrosplenial cortex (RSC) and the ventral forebrain. Remarkably, every neuron that exhibited immunopositivity for SST also displayed positivity for RFP in all these regions (Fig. 1A-C), being almost absent neurons that only expressed RFP or SST.

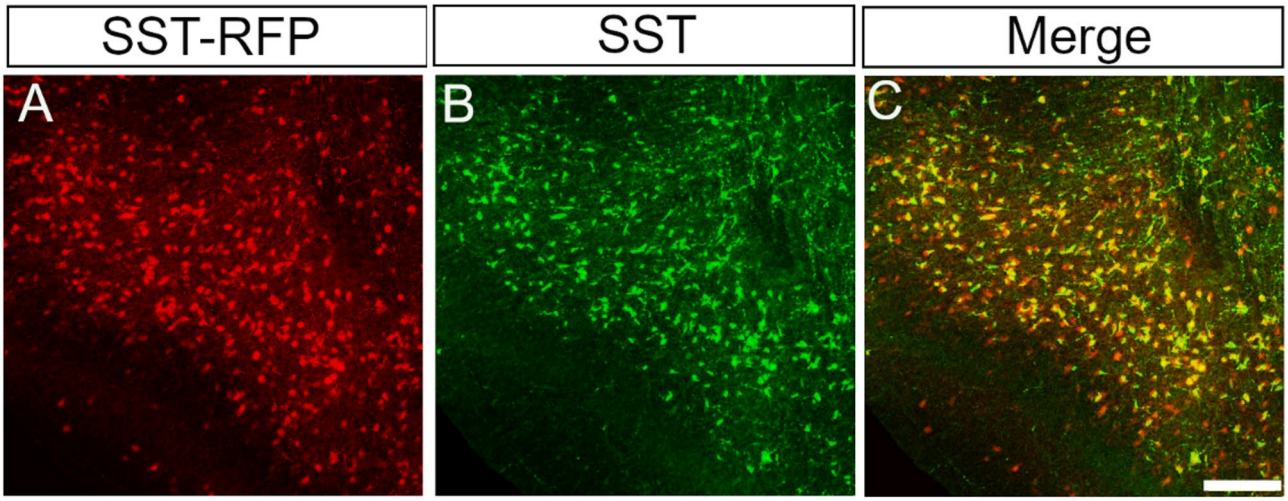

Fig. 1. SST-Cre driver specificity in the SST+ interneurons. Immunofluorescence images depicting a coronal section from a P1 mouse of the *Lis1*-SST-RFP line stained against SST and RFP of the ventral forebrain. (**A**) Image showing SST-RFP fluorescence (red). (**B**) Image showing SST immunofluorescence (green). (**C**) Fluorescence image displaying the overlay of the SST-RFP (red) and SST immunofluorescence (green). Scale bar in C (200 μm) applies to all panels.

The number and density of SST+ neurons are reduced in ACC and in the RSC of Lis1SST KO mice

To study the effect of *Lis1* inactivation selectively in SST expressing interneurons in the cingulate cortex, we assessed SST expression by immunohistochemistry in coronal sections at P30 stage. For data comparison we analyzed either CRE-negative *Lis1*fl/+ (WT; fl/+) or CRE-positive *Lis1*fl/+ (CRE; fl/+) mice as control group, and Lis1SST knock-in mice (Lis1SST KO) as mutant mice. The analysis between CRE-negative Lis1fl/+ (WT; fl/+) mice and CRE-positive Lis1fl/+ (CRE; fl/+) mice did not reveal statistical differences between these two groups of animals, indicating that the presence of the Cre recombinase alone did not significantly alter interneuron numbers in the cingulate cortex.

The number and density of SST+ neurons in the anterior cingulate cortex (ACC) are shown in Fig. 2; Table 1. At P30, immunopositivity for SST was detected in all cortical layers (II-VI) of the ACC in all animals analyzed (Fig. 2B-D). Quantification of SST+ interneurons in the ACC showed a decrease in both the number and density of SST+ cells in Lis1SST KO mice compared to the controls (Fig. 2E-H; Table 1). This decrease in number or density of cells was apparent considering either the values for the whole cortex (Fig. 2E, F; Table 1; $p = 0.001$, Mann-Whitney test) or the values for individual cortical layers (Fig. 2G-H; Table 1); in the case of individual layers the decrease was significant in all layers studied (total number: $p = 0.001$ for layers 2/3, 5 and 6 for WT; fl/+ and CRE; fl/+ vs. Lis1SST KO ; density: $p = 0.001$ for all layers for WT; fl/+ and CRE; fl/+ vs. Lis1SST KO, Mann-Whitney test).

The laminar pattern of the GABAergic interneurons plays a crucial role in cortical information processing. As described above, we observed a decrease of SST+ cells in the ACC of Lis1SST KO mice. Then, we examined the possibility that the distribution of GABAergic interneurons could be altered in Lis1SST KO mice. To test this

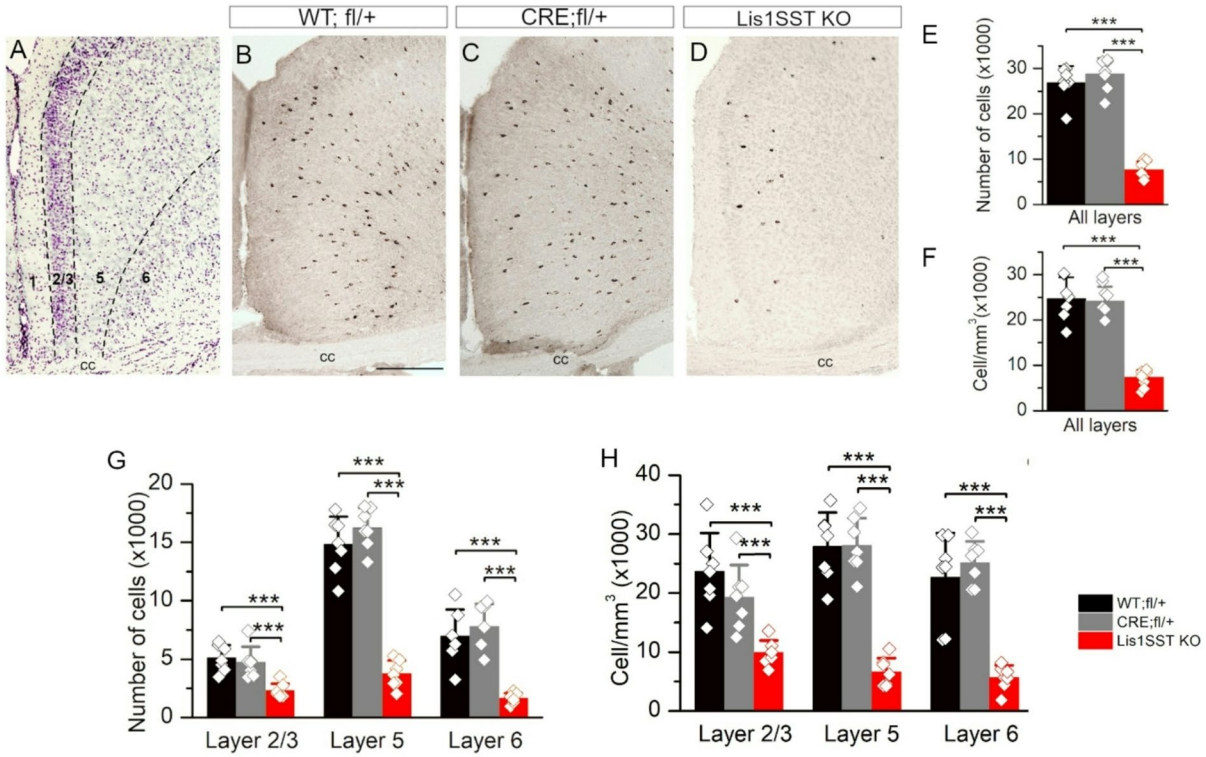

Fig. 2. Number and density of SST+ neurons in control and mutant anterior cingulate cortex (ACC). A; Representative image stained with cresyl violet showing the boundaries of the cortical layers (I-VI); cresyl violet staining was used to identify the anatomical boundaries of the cortical layers. B-D; Representative photomicrographs of coronal sections taken through the anterior cingulate cortex and processed by immunoperoxidase staining for somatostatin (SST). SST immunostaining shows a decrease in SST+ interneurons in Lis1SST KO mice versus control mice (WT; fl/+, CRE; fl/+). Limits between cortical layers marked in each panel; cc: corpus callosum. E-H; histograms showing the number and density of SST labeled neurons in the ACC. Cell density given as cells/mm3 (x1000); all data given as mean ± s.d. Symbols: values from individual brain hemispheres. E, total number of SST+ cells detected (x1000) in all cortical layers studied (average ± SD; $n = 8$; for exact values consult Table 1). F, average neuron density in all cortical layers studied (mean ± SD; $n = 7$; for exact values consult Table 1). G, number of SST+ neurons detected in individual layers (average ± SD; $n = 7$; for exact values consult Table 1); H, cell density in individual layers (mean ± SD; $n = 7$; for exact values consult Table 1). All comparisons made with the Mann-Whitney test (rank sum test); *** $p < 0.001$ (for exact values see Table 1). Scale Bar in B (200 μm) applies to panels C-D.

ACA						RSC			
Total number									
Layer	*Genotype*	*Mean*[#]	*SD*	*p, Mann-Whitney*		*Mean*	*SD*	*p, Mann-Whitney*	
				WT; fl/+	CRE; fl/+			WT; fl/+	CRE; fl/+
Layer 2/3	WT; fl/+	5.1	1.1			11.1	2.6		
	CRE; fl/+	4.7	1.3	0.604		10.9	2.1	1	
	Lis1SST KO	2.7	0.7	0.001***	0.001***	4.5	1.6	0.001***	0.001***
Layer 5	WT; fl/+	14.7	2.4			21.6	3.6		
	CRE; fl/+	16.2	1.7	0.259		22.4	5.2	0.613	
	Lis1SST KO	6.2	2.1	0.001***	0.001***	6.2	2.1	0.001***	0.001***
Layer 6	WT; fl/+	7	2.3			10.5	2.7		
	CRE; fl/+	7.7	1.9	0.71		10.2	2.7	0.779	
	Lis1SST KO	2.7	0.7	0.001***	0.001***	2.8	0.7	0.001***	0.001***
All layers	WT; fl/+	26.8	3.7			43.3	7.2		
	CRE; fl/+	28.6	3.5	0.383		43.4	9	0.867	
	Lis1SST KO	13.3	2.1	0.001***	0.001***	13.3	2.1	0.001***	0.001***
Density									
Layer 2/3	WT; fl/+	26.4	5.6			26.8	5.6		
	CRE; fl/+	24.7	5.2	0.259		24.7	5.2	0.536	
	Lis1SST KO	12.3	4.5	0.001**	0.001**	12.3	4.5	0.001***	0.001***
Layer 5	WT; fl/+	26.4	5.2			26.4	5.2		
	CRE; fl/+	27.1	7.3	0.902		27.1	7.3	0.779	
	Lis1SST KO	8.3	2.4	0.001***	0.001**	8.4	2.4	0.001***	0.001***
Layer 6	WT; fl/+	23.7	6.6			23.7	6.6		
	CRE; fl/+	22.5	5.7	0.71		22.5	5.7	0.694	
	Lis1SST KO	6.9	2	0.001***	0.001**	6.9	2	0.001***	0.001***
All layers	WT; fl/+	25.7	5			25.7	5		
	CRE; fl/+	25.2	5.9	0.805		25.2	5.9	0.955	
	Lis1SST KO	9.2	2.2	0.001**	0.001***	9.2	2.2	0.001***	0.001***
Volume									
Layer 2/3	WT; fl/+	0.19	0.03			0.41	0.007		
	CRE; fl/+	0.19	0.02	0.159		0.44	0.008	0.414	
	Lis1SST KO	0.21	0.03	0.209	0,899	0.37	0.01	0.734	0.39
Layer 5	WT; fl/+	0.56	0.01			0.82	0.01		
	CRE; fl/+	0.6	0.007	0.863		0.83	0.02	0.514	
	Lis1SST KO	0.75	0.02	0.169	0.152	0.74	0.01	0.86	0.471
Layer 6	WT; fl/+	0.3	0.01			0.44	0.01		
	CRE; fl/+	0.34	0.01	0.866		0.45	0.007	0.959	
	Lis1SST KO	0.39	0.01	0.73	0.877	0.41	0.008	0.56	0.423
All layers	WT; fl/+	1.04	0.13			1.68	0.02		
	CRE; fl/+	1.13	0.22	0.652		1.72	0.03	0.543	
	Lis1SST KO	1.45	0.24	0.361	0.227	1.45	0.03	0.674	0.377

Table 1. Descriptive statics and comparison of SST+ populations at P30 in ACC and RSC. *n*= 5 for CRE; fl/+ and Lis1SST KO and *n*= 6 for WT; fl/+. Statistical significance was considered at a p-value of less than 0.05, denoted as *p<0.05, **p<0.01 and ***p<0.001.[#] Mean: number of cells or density (mm^3) x1000.

possibility, we compared the distribution of density of SST-positive GABAergic interneurons between cortical layers (layers 2/3, 5 and 6) of the controls and the Lis1SST KO mice.

The analysis of the distribution (laminar pattern) of SST-positive interneurons among layers 2/3, 5 and 6 of CRE-negative Lis1fl/+ (WT; fl/+) does not reveal statistical differences in the ACC. We used the values of cell density in cortical layers from Fig. 2H to analyze and compare the laminar pattern of the distribution of SST+ neurons between controls and mutant cortices. In the CRE-positive Lis1fl/+ (CRE; fl/+) mice, the neuron density in layer 2/3 was significantly lower than in layers 5 and 6 ($p < 0.05$, Kruskal-Wallis test, with post-hoc Tukey test); this suggest that in control animals SST+ neurons are placed preferentially in deep layers. In contrast, in the Lis1SST KO mice the neurons density in layer 6 was significantly lower than in layers 2/3 and 5 ($p < 0.05$, Kruskal-Wallis test, with post-hoc Tukey test), suggesting that in these animals the neurons gradient was inverted, and SST+ neurons were placed preferentially in superficial layers.

In the retrosplenial cortex (RSC) our findings were similar to ACC (Fig. 3; Table 1). As in ACC, at P30, immunopositivity for SST was detected in all cortical layers (II-VI) of the RSC in all animals analyzed (Fig. 3B-D). In the RSC we detected a decrease in both the number and density of SST+ cells in Lis1SST KO mice compared to the controls (Fig. 3E-H). This decrease in number or density of cells was significant either considering the values for the whole cortex (Fig. 3E-F; Table 1; $p = 0.001$ for WT; fl/+ vs. Lis1SST KO and $p = 0.001$ for CRE; fl/+ vs. Lis1SST KO for total number and density, Mann-Whitney test) or the values for individual cortical layers (Fig. 3G-H); in the case of individual layers the decrease in cell number or density was significant in all layers studied (Table 1; $p = 0.001$ for WT; fl/+ vs. Lis1SSTKO and $p = 0.001$ for CRE; fl/+ vs. Lis1SST KO for total number and density, Mann-Whitney test).

The analysis of the distribution of SST-positive interneurons of RSC showed findings similar to ACC. The analysis of SST-positive interneuron distribution between layers 2/3, 5, and 6 in CRE-negative Lis1fl/+ (WT; fl/+) and mice CRE-positive Lis1fl/+ (CRE; fl/+) mice did not reveal statistical differences in the RSC (Fig. 3). As in the ACC, we also observed an increase in the density of SST-positive interneurons in the superficial layer (layer 2/3) of the mutants. This increase in cell density was significant between layers 2/3 and 6 in the RSC (Fig. 3; $p < 0.05$, Kruskal-Wallis test with post-hoc Tukey test).

The prenatal migration of SST+ interneurons tangential migration is altered in Lis1SST KO animals

The reduced density of SST+ neurons found in the postnatal cortex of Lis1 SST KO animals suggest that the proliferation and / or the migration of these neurons during the cortical development may be altered. First, we

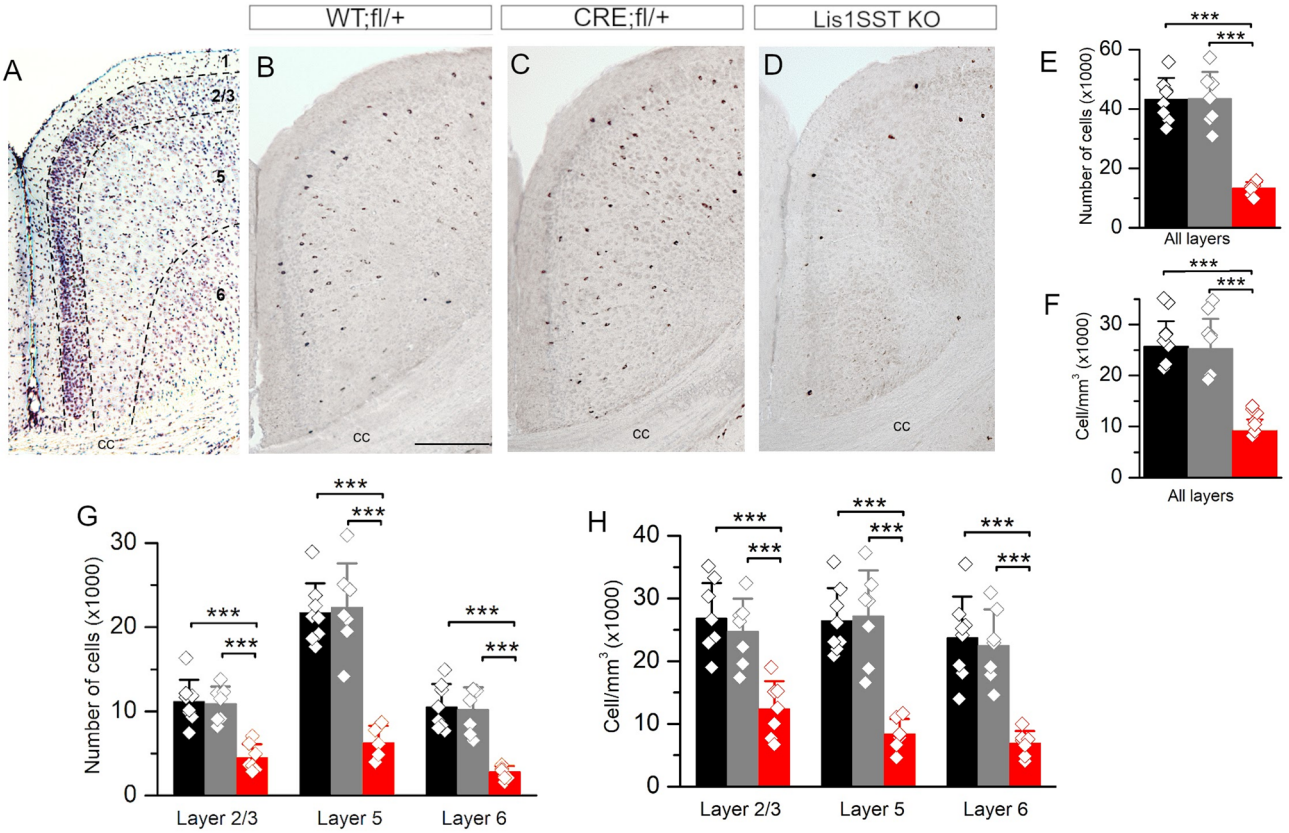

Fig. 3. Number and distributions of SST + neurons in control and mutant Retrosplenial cortex (RSC) A; Representative image stained with cresyl violet showing the boundaries of the cortical layers (I-VI); cresyl violet staining was used to identify the anatomical boundaries of the cortical layers. B-D; Photomicrographs of coronal sections taken through the anterior cingulate cortex and processed by immunoperoxidase staining for somatostatin (SST). SST immunostaining shows a decrease in SST+ interneurons in Lis1SST KO mice versus control mice (WT; fl/+, CRE; fl/+). Limits between cortical layers marked in each panel; cc: corpus callosum. E-H; histograms showing the number and distributions of SST labeled neurons in the RSC. Cell density given as cells / mm3; all data given as mean ± s.d. Symbols: values from individual brain hemispheres. E, total number of SST+ cells (x1000) detected in all cortical layers studied; (average ± SD; $n = 8$; for exact values consult Table 1). F, average neuron density (cells/mm3 × 1000) in all cortical layers studied (average ± SD; $n = 8$; for exact values consult Table 1). G, number of SST+ neurons detected in individual layers (average ± SD; $n = 8$; for exact values consult Table 1). H, cell density in individual layers (average ± SD; $n = 8$; for exact values consult Table 1). All comparisons made with the Mann-Whitney test (rank sum test); *** $p < 0.001$ (for exact values see Table 1). Scale Bar in B (200 µm) applies to panels C-D.

analyzed the neuronal proliferation at the medial ganglionic eminence, where most of the SST+ neurons are generated, although it is known that SST+ interneurons divide in the ventricular zone[42]. Once these interneurons exit the cell cycle, they migrate into the subpallial mantle zone, where the first expression of the Sst gene is detected[42–44]. Sst-lineage cells are already postmitotic at the time Sst-Cre becomes active; therefore, Lis1 deletion in this lineage cannot directly influence MGE progenitor proliferation, consistent with studies showing that Sst interneuron precursors exit the cell cycle before initiating Sst expression[16,45]. Nonetheless, we examined Ki67 immunoreactivity and confirmed the absence of proliferative activity within the Sst-Cre lineage. We performed double immunohistochemistry with anti-RFP and anti-Ki67 antibodies (the latter is a proliferation marker; [46]and we did not detect any degree of co-labeling (Fig. 4), which suggests that cell proliferation should not be affected by the deletion of *Lis1* when the *Sst* gene is expressed.

Inhibitory interneurons are primarily generated in the ganglionic eminences and the preoptic area, and follow a long path until reaching their final destination in the cortex[21,47]. In particular, SST+ interneurons are born in the medial ganglionic eminence (MGE) between embryonic days E10.5 and E16.5, with a maximum at E15.5 [48,49]. During tangential migration, SST+ interneurons are organized in two streams: the marginal zone (MZ) stream and the subventricular zone (SVZ) stream[21]. To analyze whether tangential migration could be affected in Lis1SST KO; RFP mice, we studied brains from Lis1SST KO; RFP mice at embryonic stages E14.5 and E16.5; the expression of the RFP protein when SST promoter is activated in these mice allowed us to follow SST+ interneurons during embryonic development. Figure 5 shows the tangential migration of SST+ neurons at E14.5 and E16.5 stages.

An initial analysis revealed a reduction in the number of migrating SST-RFP interneurons in the cortex at both stages, particularly noticeable in the dorso-medial areas (Fig. 5B-D, F-H). To corroborate this qualitative observation, we conducted a quantitative analysis. This was done counting RFP expressing cells in a rectangular region of 250 µm wide and covering the whole cortex. The same rectangular region size was used for analysis at both E14.5 and E16.5 (Fig. 5A, E). SST-RFP interneurons were counted in the marginal zone (MZ), cortical plate (CP), subplate (SP), intermediate zone (IZ), and subventricular zone (SVZ). The analysis between control mice (CRE; RFP) and heterozygous mice (CRE; fl/+; RFP) mice did not reveal any statistical significant differences between these two groups. Neuron quantification at E14.5 showed a significant decrease in the number of SST^{+} neurons in the MZ, IZ, and SVZ of mutant mice (Fig. 5I; Table 2; for CRE; RFP vs. Lis1 SST KO; RFP: $p = 0.002$ in MZ; $p = 0.035$ in IZ and $p = 0.026$ in SVZ; Student's t-test), which was similarly observed when comparing heterozygous and mutant mice (Fig. 5I; Table 2; CRE; fl/+; RFP vs. Lis1 SST KO; RFP: $p = 0.004$ in MZ; $p = 0.008$ in IZ and $p = 0.008$ in SVZ; Student's t-test). At E16.5, we also detected a significant reduction in the number of SST^{+} neurons in the MZ and SP of mutant mice compared with controls (Fig. 5J; Table 2; for CRE; RFP vs. Lis1 SST KO; RFP: $p = 0.026$ in MZ; and $p = 0.001$ in SP; Student's t-test) and compared with heterozygous mice (Fig. 5J; Table 2; for CRE; fl/+; RFP vs. Lis1 SST KO; RFP: $p = 0.005$ in MZ; and $p = 0.01$ in SP; Student's t-test). These findings indicate an altered migration of SST-RFP neurons in the mutant prenatal cortex that is clear since at least the E14.5 stage.

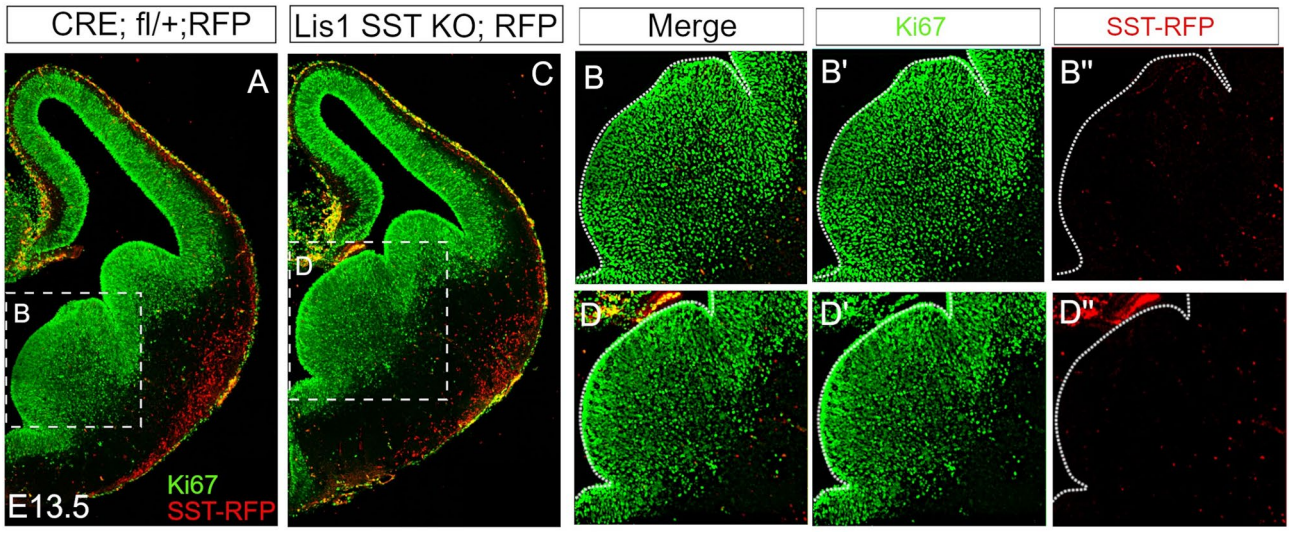

Fig. 4. Cell proliferation in the medial ganglionic eminence. A-C; Coronal sections showing immunostaining against Ki67 (green) or RFP (red) at E13.5. Representative coronal sections of a CRE; fl/+; RFP mouse (A) and a Lis1SST KO; RFP mouse (C). B and D are close-ups of the boxed areas in A and C, respectively, corresponding to the medial ganglionic eminences, where SST+ interneurons are born. B corresponds to the merged image, with B′ showing the Ki67 (green) and B″ showing the SST–RFP (red). Similarly, D corresponds to the merged image, with D′ showing the Ki67 (green) and D″ showing the SST–RFP (red).

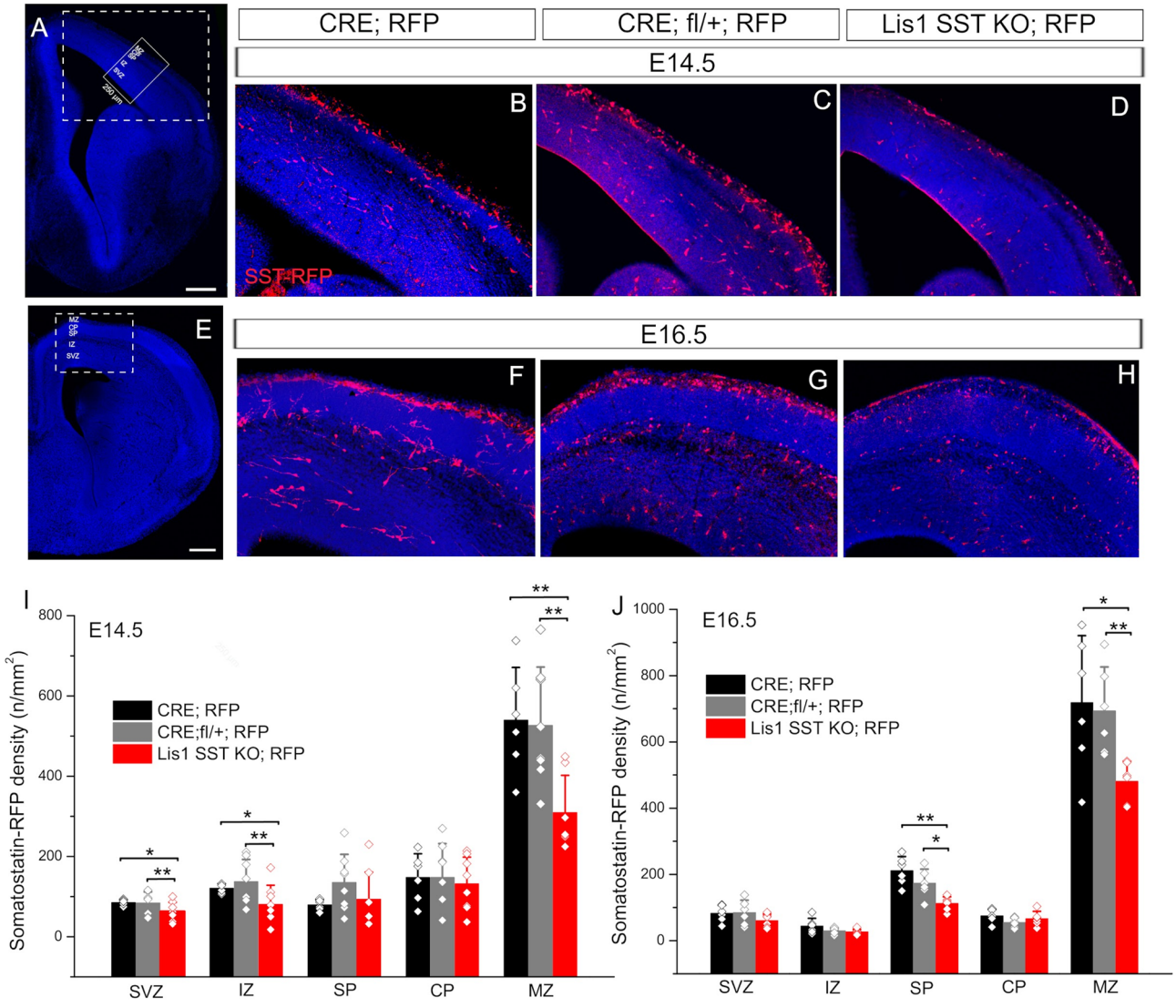

Fig. 5. Tangential migration of SST-positive interneurons in Lis1SST KO; RFP mice at E14.5 and E16.5 stages. Representative images of the developing cortex from coronal sections of E14.5 (A-D) or E16.5 (D-H) CRE; RFP; CRE; fl/+; RFP or Lis1SST KO; RFP embryos immunostained against RFP (red) and counterstained with DAPI (blue). Dashed squares in A and E (only DAPI staining) indicate the approximate area shown enlarged in panels B-D and F-H respectively. The small rectangles in A and E show the area used to count RFP neurons. I, J, density (neurons / mm2) of RFP-labeled neurons in cortical layers at E14.5 stage (I) and E16.5 stage (J); values given as mean ± s.d.; $n = 8$ (I) or $n = 6$ (J); Student's t-test; $^{*}p < 0.05$, $^{**}p < 0.01$; for exact values see Table 2). Scale Bar in panels A and E measures 200 µm.

The morphology of migrating SST+ neurons is altered in *Lis1SST KO; RFP* animals

We next analyzed the morphology of migrating SST+ interneurons. The morphological analysis was made after enhancing the RFP fluorescent signal in those neurons selected for morphological analysis with immunohistochemistry against RFP performed at the embryonic stage E15.5. Interneurons migrating tangentially through the intermediate zone were selected for morphological analysis once they reached the dorsal pallium. In addition to a reduction in the number of migrating cells reported above, *Lis1* silencing during the development of SST+ interneurons resulted in morphological abnormalities in the leading processes and its branches as well as in the soma of migrating neurons (Fig. 6). For the morphological analysis, we selected cells from six animals per condition in both control and mutant groups, ensuring consistent and representative sampling across all experimental groups. In control mice, most migrating neurons showed a leading process with a single branching node and two branches (31 out of 36 neurons: 86.1%; the remaining neurons showed a non-branching leading process); in contrast, in mutant animals the number of neurons showing a branched leading process was much lower (21 out of 36; 58.3%), and this difference was statistically significant ($\chi^2(1, N = 72) = 6.92$, $p = 0.009$). Our morphological analysis of migrating neurons revealed significant differences in both the length of the leading process and its branches and in the size and shape of the soma. The length of the leading process was shorter in

E14.5								
	CRE; RFP		CRE; fl/+;RFP		Lis1SST KO; RFP			
	Mean	*SD*	*Mean*	*SD*	*Mean*	*SD*	*p, Student's t test CRE; RFP vs. Lis1SST KO; RFP*	*p, Student's t test CRE; fl/+;RFP vs. Lis1SST KO; RFP*
SVZ	85	8	84	28	63	23	0,026*	0.008**
IZ	121	12	137	55	80	47	0,035*	0.008**
SP	79	13	135	70	93	68	0,059	0.247
CP	148	59	147	84	131	66	0,657	0.641
MZ	539	131	526	145	309	93	0,002**	0.004**
E16.5								
	CRE; RFP		CRE; fl/+;RFP		Lis1SST KO; RFP			
	Mean	*SD*	*Mean*	*SD*	*Mean*	*SD*	*p, Student's t test CRE; RFP vs. Lis1SST KO; RFP*	*p, Student's t test CRE; fl/+;RFP vs. Lis1SST KO; RFP*
SVZ	82	25	84	37	60	20	0,123	0.196
IZ	44	23	28	8	26	8	0,113	0.606
SP	211	43	172	42	112	20	0,001**	0.01*
CP	74	20	54	14	66	22	0,532	0.293
MZ	718	202	693	133	480	61	0,026*	0.005**

Table 2. Descriptive statistics and comparison of migrating cells across Genotypes. *n*=8 for E14. 5 and *n*=6 for E16.5 (CRE; RFP, CRE; fl/+;RFP and Lis1SST KO; RFP). Statistical significance was considered at a p-value of less than 0.05, denoted as *p<0.05, **p<0.01 and ***p<0.001.

Lis1SST KO; RFP mice compared to controls; the length of the branches was also shorter in Lis1SST KO; RFP mice (Figs. 6-D).

Quantitative analysis revealed that Lis1SST KO; RFP interneurons displayed a significant reduction in soma size compared to controls, as measured by the somatic perimeter (Fig. 6E). The shape of the soma was also different in Lis1SST KO; RFP interneurons, being more compact and more rounded, as indicated by the aspect ratio, roundness and compactness (Fig. 6F-H).

These findings suggest that the absence of the *Lis1* gene in SST+ interneurons disrupts normal morphological development, resulting in shorter leading processes with fewer and shorter branches, as well as a more rounded and compact soma with reduced perimeter.

SST+ interneurons of Lis1SST KO experience a halt in their tangential migratory stream

Since interneuron proliferation in the ganglionic eminence is not affected but the number of migrating neurons in the dorsal embryonic cortex is largely decreased, we hypothesized that migrating neurons suffer some kind of accumulation at the basal forebrain, the area through which migrating neurons transitate in their way from the ganglionic eminence to the developing dorsal cortex. We focused our analysis on the basal forebrain in coronal sections of E15.5 (Fig. 7). Since we have observed a low number of migrant neurons as early as E14.5, we anticipated the accumulation of migrant neurons in the basal forebrain one day later, at E15.5. To define our area of interest, we draw two parallel lines from the medial and lateral vertices of the ventricle, extending from the neuroepithelium to the pial surface. We then analyzed the area between the neuroepithelium and the pial surface, bounded by these lines (Fig. 7A-D). Given the high density of labeling in this basal region, we decided to quantify the fractional area labeled by SST-RFP relative to the previously defined area of interest. Our analysis of the fractional area occupied by SST-RFP, revealed a stalling of SST+ interneurons in the basal forebrain in Lis1SST KO; RFP mice (Fig. 7E).

The quantification using the AFF probe revealed that the area fraction occupied by SST-RFP in the basal region was larger in the Lis1SST KO; RFP compared to controls (Fig. 7E), indicating an accumulation of migrating neurons in mutant mice. The area fraction occupied by SST-RFP in the cortex was larger in the controls compared to Lis1SST KO; RFP (Fig. 7E). No significant differences were observed in the overall area fraction occupied by SST-RFP in the basal forebrain and cortex (Fig. 7F).

The accumulation of SST+ interneurons in the ventral telencephalon suggests that these cells may be undergoing cell death due to their failure to reach their final destination. To test this hypothesis, we performed immunohistochemistry to detect cells expressing Caspase-3 at the P1 postnatal stage. We observed fewer Caspase-3 + cells in the ventral telencephalon of control mice compared to Lis1SST KO mice (Fig. 8A-C').

To quantify this observation, we defined a quadrangular region using the ventral horn of the lateral ventricle and the ventral end of the external capsule (ec) as reference points. The dorsal side of the rectangle was drawn by connecting these two points, while the remaining sides extended from these points to the pial surface of the ventral telencephalon (Fig. 8A). We then applied stereological methods to estimate the number of Caspase-3 + cells in each group. Our analysis revealed a statistically significant increase in the number of Caspase-3 + cells in Lis1SST KO mice compared to controls (Fig. 8D).

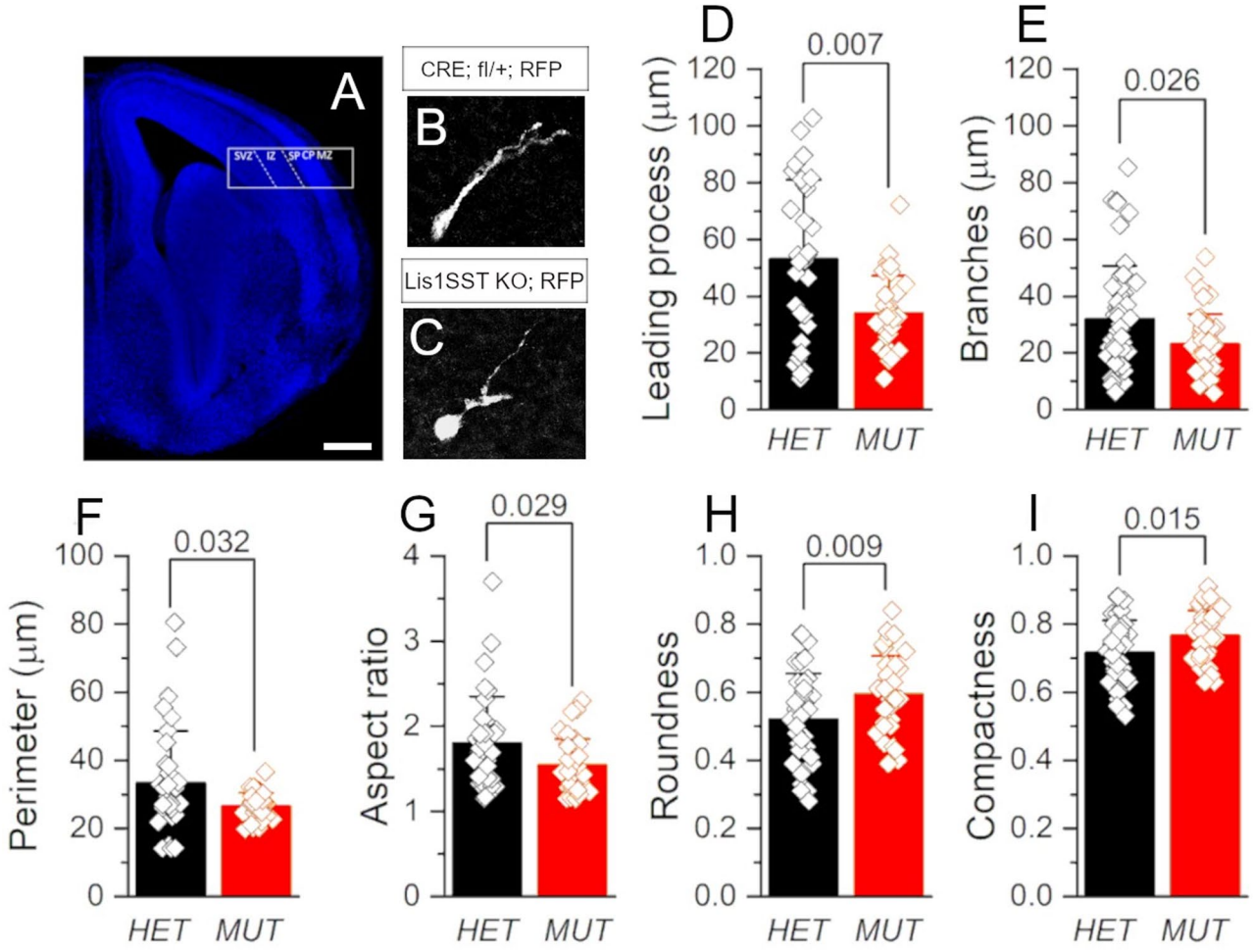

Fig. 6. Morphological defects observed in tangentially migrating SST-positive interneurons of Lis1SST KO; RFP mice at E15.5. A: Representative coronal section of the developing cortex at E15.5. The square indicates the region in which morphological analysis was performed. Dashed lines delineate the intermediate zone where SST-RFP interneurons were analyzed. B, C; Representative images of SST-RFP interneurons located in the intermediate zone in CRE; fl/+; RFP and Lis1SST KO; RFP brain. D, E; Histograms showing the length of the leading process (D; CRE; fl/+; RFP 53.15 ± 27.91 µm, $n = 30$; Lis1SST KO; RFP 33.94 ± 13.30 µm, $n = 30$) and branch length (E; CRE; fl/+; RFP 32.02 ± 18.72 µm, $n = 54$; Lis1SST KO; RFP 23,28 ± 10.41 µm, $n = 42$). F, Somatic perimeter length (CRE; fl/+;RFP 33.39 ± 15.15 µm, $n = 36$; Lis1SST KO; RFP 26.52 ± 3.93 µm, $n = 36$). G-I, aspect ratio (G; CRE; fl/+;RFP 1.80 ± 0.54, $n = 36$; Lis1SST KO; RFP brain 1.55 ± 0.31, $n = 36$), roundness (H; CRE; fl/+;RFP 0.52 ± 0.14, $n = 36$; Lis1SST KO; RFP brain 0.60 ± 0.11, $n = 36$) and compactness (I; CRE; fl/+;RFP 0.72 ± 0.09, $n = 36$; Lis1SST KO; RFP brain 0.77 ± 0.07, $n = 36$) of the soma. All data given as mean ± s.d; symbols in the histograms are the values from individual neurons. Comparisons with the Mann-Whitney rank sum test (p-value given above each histogram). Scale Bar in panels A measures 200 µm and in panels B and C 20 µm.

These findings suggest that the absence of the *Lis1* gene in SST+ interneurons the tangential migration of these neurons is disrupted, leading to their accumulation and subsequent cell death in the ventral telencephalon during early development.

A; Schematic representation of a coronal mouse brain section illustrating the region selected for quantitative analysis of Caspase-3 + cells. B-C; Coronal sections of a CRE; fl/+ brain (B) and a Lis1SST KO brain (C) immunostained for Caspase-3. B'-C'; Higher magnification images of the boxed regions in (B) and (C) respectively. D; Histogram showing the quantification of Caspase-3 + cell density (mean ± SD; $n = 6$; CRE; fl/+ = 1458 ± 790; Lis1SST KO = 2404 ± 1346; Student's t-test, $p = 0.037$). Scale bar in panel B applies to panels B, C (500 µm) and to panels B', C' (125 µm). (Abbreviations: ac: anterior commissure; cc: corpus callosum; CP: caudoputamen; CTX-cortex; ec: external capsule; se: septum).

Discussion

In the present study, we analyzed the effect of *Lis1* mutation in SST+ interneurons in the mouse cingulate cortex. Our findings indicate that deletion of the *Lis1* gene during the development of SST+ interneurons, specifically

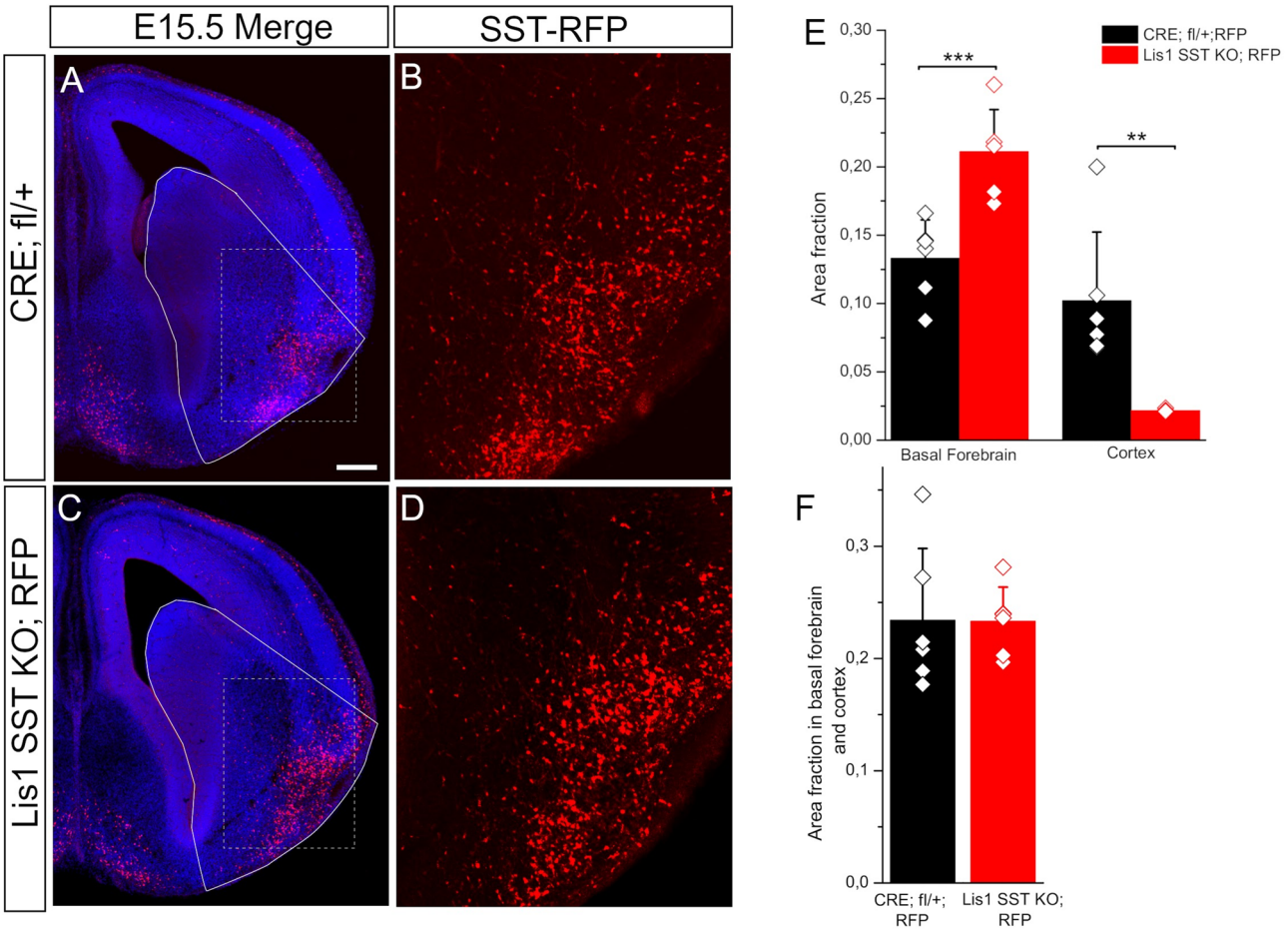

Fig. 7. SST-positive interneurons accumulate in the basal forebrain during early embryonic development. A, C; Coronal sections of a CRE; fl/+; RFP brain (A) and a Lis1SST KO; RFP brain immunostained for RFP and counterstained with DAPI. B, D; Higher magnification images of the boxed area in (A) and (C) are shown in B and D (RFP immunostaining). E; The histogram shows the quantification of the fractional area occupied by RFP positive neurons in the basal forebrain (mean ± SD; $n = 6$. CRE; fl/+ 0.133 ± 0.01; Lis1SST KO 0.21 ± 0.01, Student's t-test, $p = 0.0005$) and in the cortex (mean ± SD; $n = 6$. CRE; fl/+ 0.102 ± 0.05; Lis1SST KO 0.021 ± 0.001, Student's t-test, $p = 0.002$). F; The histogram represents the quantification of the fractional area occupied by RFP positive neurons in the basal forebrain and cortex (mean ± SD; $n = 6$. CRE; fl/+ 0.234 ± 0.06; Lis1SST KO 0.233 ± 0.03, Student's t-test, $p = 0.952$). Scale bar in panel A applies to panels A, C (500 µm) and to panels B, D (200 µm).

reduces the number of SST+ interneurons in the cingulate cortex in young mutant mice. Our results also revealed that *Lis1* gene deletion strongly affects tangential migration of SST+ interneurons. These results demonstrate the SST+ interneurons populating the cingulate cortex are affected by the lack of *Lis1* during development, supporting the idea that the *Lis1* effect is cell autonomous. According to our observations *Lis1* is necessary for the proper development of SST+ interneurons.

Morphological consequences of Lis1 ablation in the cingulate cortex

Disruptions in brain development often play a central role in various psychiatric disorders and intellectual disabilities. The identification of genes contributing to these disorders in humans, such as *Lis1*, has shed light on this intricate relationship[12,50–52]. *Lis1* has been implicated in neurobehavioral disorders like autism, schizophrenia (SCZ), and human psychosis. The role of the *Lis1* gene in the development and function of the GABAergic system has been suggested using hypomorphic mutation of the *Lis1* allele (sLis1) and the heterozygous mutation (Lis1+/-) [9,12,53–56]. Previous studies revealed a disorganized hippocampal area CA1 in Lis1+/- mice, characterized by a selective displacement parvalbumin- and somatostatin- positive interneurons, leading to functional changes in neural circuitry[5,8]. Moreover, they observed that interneuron migration is slowed in *Lis1* mutant mice, likely disrupting the synaptic integration of these cells.

In previous studies in our laboratory, we observed a reduction of GABAergic interneurons, including glutamate decarboxylase 1, parvalbumin and calretinin in the ACA in the young stages of *Lis1/sLis1* mutant mice[12]. In this study, we observed similar results regarding SST+ interneurons in the cingulate cortex. The total number of these cells was severely reduced in Lis1SST KO. Furthermore, density analysis revealed a decrease

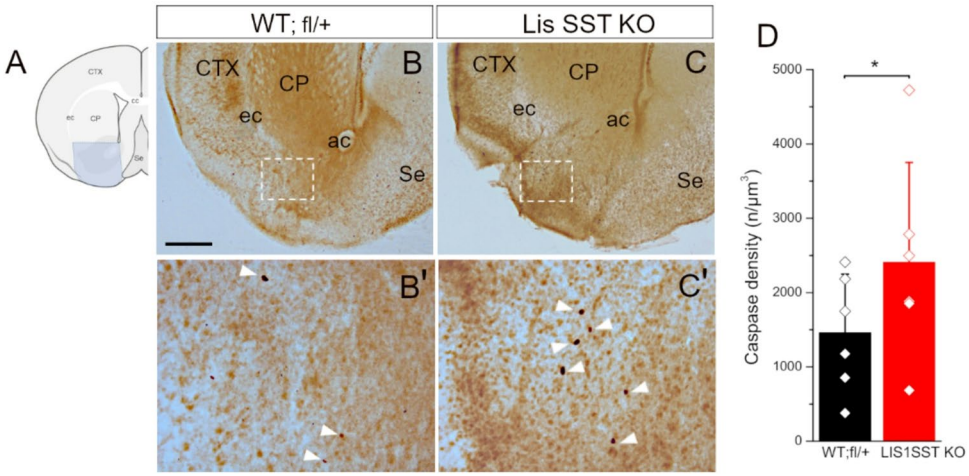

Fig. 8. Increased Caspase-3 + cell death in the ventral telencephalon of Lis1SST KO mice.

in the entire ACC and RSC, as well as by layers. Unbiased stereological estimations of volume of ACC and RSC layers were carried out. No volume reduction was detected in the entire ACC and RSC or by layers, ruling out the influence of volume changes when comparing density (see Table 1 for details). By specifically deleting *Lis1* in SST+ interneurons, we demonstrate that *Lis1* is involved in the proper development of SST+ interneurons. Moreover, we observed a distinct alteration in the distribution of SST+ interneurons across the cortical layers. In mutant mice, layer 2/3 exhibited a higher density of SST+ interneurons compared to layer 6. One possible explanation is that Lis1 plays a role in the radial migratory route that SST+ interneurons follow upon reaching the cortex. However, further experiments would be necessary to clarify this point. Indeed, previous studies have reported cortical dysplasia when the Lis1 gene is mutated[53,57]. Furthermore, using extracellular field potential and intracellular recordings in brain slices of the cingulate cortex, we observed that the dysfunction of the *Lis1* gene causes abnormalities in the properties of epileptiform discharges and in their propagation along the layer 2/3 [58]. Therefore, the severe reduction of SST+ interneurons in the cingulate cortex could also alter the limbic circuitry, producing an excitatory-inhibitory imbalance. A decrease in SST expression in the human brain has been implicated in various neurodegenerative disorders[59]. The reduction of SST expression is related to a decrease in the number of SST+ interneurons in several neurodegenerative disorders, such as a reduction in the frontal cortex and hippocampus in Alzheimer's disease[60,61], in the cortex in Parkinson's disease[62], in the striatum in Huntington's disease[63] and in the hippocampus in SCZ[64]. Furthermore, an association between some lissencephaly-related genes and both SCZ and bipolar disorder has been reported[12,52,65]. In fact, the interaction of LIS1 with other proteins considered as risk factors for major mental illness has been proposed as critical for developing SCZ and related psychiatric disorders[66].

Here, we demonstrate that the ablation of *Lis1* in SST+ interneurons severely affects the number of these cells in the cingulate cortex, suggesting important physiological consequences in its proper functioning that could be related to neuropathological disorders.

Role of Lis1 in the migration of SST-interneurons

SST-interneurons, characterized by somatostatin expression, form the second largest class of cortical interneurons and favor dendritic synapse formation[21]. SST+ interneurons originate from the dorsal and intermediate regions of the MGE between the embryonic days E10.5 and E16.5 [21,48]. They arise from apical progenitors that undergo division along the VZ [42] before embarking on tangential migration to the cortex via two primary routes: the MZ, predominantly followed by Martinotti cells, and the SVZ, favored by non-Martinotti cells[18]. In our study, we examined the impact of *Lis1* gene deletion on the migration of SST+ interneurons during development. Our findings revealed a reduction in the total number of migrating SST+ interneurons at both E14.5 and E16.5 stages in *Lis1SST* KO animals compared to controls. Analysis of distinct developing cortical layers indicated that the number of SST+ interneurons migrating through the main migratory routes, the SVZ and the MZ, was disrupted during the stages examined. Crucially, migration through the MZ is a key route for the tangential dispersion of late-born interneurons (Tanaka et al., 2009), and SST+ cells utilizing this superficial stream are fate-determined to become Calb2 + Martinotti cells (Lim et al., 2018). Therefore, the concurrent blockade of the deep (SVZ) and superficial (MZ) streams suggests that both Martinotti and non-Martinotti cells were equally affected by the *Lis1* deletion. However, we observed a higher density of SST+ interneurons in layer 2/3 compared to layer 6 in Lis1SST KO animals. This suggests that the absence of Lis1 may impair the outside-inside radial migration of Martinotti cells once they reach the cortex via the MZ route. The diminished presence of migrating SST+ interneurons in the cortex of Lis1SST KO animals underscores the crucial role of *Lis1* in this developmental process.

During cell migration, microtubules play a critical role in the cytoskeleton reorganization, with several microtubule-associated proteins such as doublecortin and LIS1 being implicated in microtubule organization and regulation cell migration[67–69]. The regulatory interaction between LIS1 and the cytoplasmic dynein is pivotal for

its cellular functions, with *Lis1* gene deletion known to affect neuronal migration, progenitor proliferation, and nucleokinesis[1,70]. The role of *Lis1* in radial migration during cortex development has been well-established. It has been demonstrated that alterations in *Lis1* dosage lead to cortical lamination defects and layer disorganization in the hippocampus[3,9]. Reduced levels of *Lis1* result in weaker coupling between the centrosome and nucleus, thereby affecting nuclear translocation and, consequently, neural migration and positioning during cortical development[9,71].

Moreover, *Lis1* appears to be essential for proper tangential migration, as demonstrated in heterozygous mice (*Lis1*+/−), where this process is impaired due to reduced nuclear translocation velocity and abnormal dynamics of both leading process branching and extension[72–74].

In our study, SST+ interneurons from Lis1SST KO mice exhibited smaller and more rounded somata compared to controls, likely reflecting delayed nuclear—and consequently somatic—translocation, consistent with previous reports[72,74]. While *Lis1*+/− interneurons display an elongated leading process and reduced branching complexity[72], Lis1SST KO SST+ interneurons showed a marked reduction in both leading process length and number of branches. These results suggest that complete *Lis1* ablation has distinct morphological consequences compared to haploinsufficiency. In line with this, a previous study reported that *Lis1*-deficient neurons exhibit shorter leading processes than those observed in wild-type or heterozygous conditions[75]. Altogether, our findings support a dose-dependent role for *Lis1* in regulating the morphology of the leading process, highlighting a complex relationship between *Lis1* expression levels and interneuron migratory behavior.

However, the question of whether the effect of *Lis1* is cell autonomous remained unresolved. While radial migration defects resulting from *Lis1* mutations are believed to be cell autonomous[3,76], alterations in tangential migration are thought to be primarily cell autonomous but may also involve non-cell-autonomous factors[72]. Interestingly, our approach of selectively deleting *Lis1* from SST+ cells helps clarify that the role of *Lis1* in tangential migration is in fact cell autonomous.

Despite the known impact of *Lis1* deficits on proliferation, this process should remain intact in our mouse model. We utilized a mouse model in which *Lis1* is deleted specifically in cells expressing the *Sst* gene, starting around the embryonic stage E13.5. SST+ interneuron precursors begin expressing the *Sst* gene just before starting tangential migration. Therefore, our mutant brain model contains postmitotic Lis1SST + KO interneurons. Our results suggest that SST+ interneurons divide correctly, but the deficiency of *Lis1* impairs tangential migration along all migratory routes, leading to a significant decrease in SST+ interneurons in the adult brain. In fact, we have observed that SST+ interneurons fail in their tangential migration and instead accumulate in the basal forebrain during early embryonic development. These findings are consistent with previous studies demonstrating that the disruption of other proteins interacting with the cytoskeleton, such as SynGAP-dopamine D1 receptor, RAC-GTPases, or Aristaless-related homeobox gene, also impairs the migration of GABAergic interneurons, resulting in their stalling in the ventral telencephalon[77–79]. Moreover, we have observed an increase in the density of cells expressing Caspase-3 suggesting that interneurons fail in their migration and consequently die in the ventral telencephalon explaining the reduction of SST+ interneurons in the cingulate cortex in adult stages. The question of whether early- and late-born Sst interneurons are differentially affected remains open, and future studies using dedicated birthdating approaches (e.g., BrdU or EdU paradigms) will be required to address this in greater detail.

Our data contribute to the better understanding of the physiopathology of neurodevelopmental pathological disorders. Both *Lis1* mutation and SST+ deficits in the cingulate cortex have been independently linked to neurological disorders. Here, we provide evidence that *Lis1* dysfunction in SST+ interneurons is associated with inadequate cell migration and a significant deficit in the young brain, which could lead to pathological outcomes. Further investigations on other types of interneurons and their functional consequences are necessary to elucidate the potential role of *Lis1* in proper cortical development and pathogenesis.

Conclusions

Our results demonstrate that the inactivation of *Lis1* in SST+ neurons causes a substantial reduction in the density of SST+ neurons in the postnatal cingulate cortex. Specifically, we observed a significant decrease in the overall cortex and individual layers of the anterior cingulate cortex, as well as in the retrosplenial cortex. During prenatal development, the tangential migration of SST+ neurons was profoundly disrupted, leading to the accumulation of SST+ neurons in the basal forebrain at E15.5. Overall, these findings indicate that Lis1 inactivation in SST+ neurons disrupts tangential migration and reduces the number of SST+ neurons in the postnatal cingulate cortex.

Methods

Animals

All animal procedures were conducted in compliance with Spanish and European Union regulations on animal welfare in experimentation, specifically adhering to Real Decreto 1201/2005 and EU Directive 2010/63/EU. All protocols were approved by the Ethical Committee for Experimental Research of the Universidad Miguel Hernández (approval number: 2021/VSC/PEA/0230). This study is reported in accordance with the ARRIVE guidelines (Animal Research: Reporting of In Vivo Experiments).

All mutant mice were maintained on the C57 genetic background. Transgenic mice expressing CRE recombinase under the control of the somatostatin (SST) promoter (SST-CRE; $Sst^{tm2.1(cre)Zjh}$/J, The Jackson Laboratory) and mice harboring the Lis1 gene flanked by flox sites (Lis1flox/flox; 129 S-Pafah1b1^{tm2Aw}/J; The Jackson Laboratory) were employed in this study. Lis1SST knock-in mice (Lis1SST KO) were generated by crossing Lis1flox/flox mice with heterozygous SST-CRE; Lis1flox/+ mice. The control group consisted of CRE-negative Lis1fl/+ (WT; fl/+) mice and CRE-positive Lis1fl/+ (CRE; fl/+) mice.

A second line was employed in this study, which, in addition to SST-CRE and flox-Lis1-flox constructs, carries a construction that leads to the expression of red fluorescent protein (RFP) only where CRE recombinase is expressed (B6.CgGt(ROSA)26Sor$^{tm14(CAG–TDTomato)Hze}$/J, The Jackson Laboratory). The Lis1SST KO; RFP mice were generated by crossing Lis1flox/flox-RFP mice with heterozygous SST-CRE; Lis1flox/+ mice. The control group consisted of CRE-positive Lis1fl/+ (CRE; fl/+;RFP) mice.

For genotyping, PCR was conducted using specific primer sets to detect the SST-CRE construct, the flox-*Lis1*-flox construct, and the RFP construct. The primer sequences are as follows: SST-CRE construct: SST Forward Primer (FP): 5′CTGGAAGACATTCACATCCTG3′; SST reverse primer (RP): 5′TATGGCAGCTGTTCCCAATAG3′; CRE FP: 5′CGGTCGATGCAACGAGTGATG3′; Cre RP: 5′AGCCTGTTTTGCACGTTCACC3′; to identify flox-*Lis1*-flox construct: FP: 5′TGAATGCATCAGAACCATGC3′; RP: 5′CCTCTACCACTAAAGCTTCTTC3′; and to identify the RFP construct: RFP FP1: 5′AAGGGAGCTGCAGTGGAGTA′3, RFP FP2 5′GGCATTAAAGCAGCGTATCC3′; RFP RP1: 5′CCGAAAATCTGTGGGAAGTC, RFP RP2: 5′CTGTTCCTGTACGGCATGG3′. These primer sets were utilized to identify the presence of each respective construct in the mice samples through PCR amplification.

The day of vaginal plug detection was designated as embryonic day 0.5 (E0.5). Animals used in developmental and histological studies ranged in age from E14.5 to P30. Postnatal day 30 (P30) mice, weighing between 12 and 17 g, were anesthetized with isoflurane (4% for induction, 1.5–2% for maintenance in oxygen) until complete loss of reflexes was confirmed, and subsequently transcardially perfused with phosphate-buffered saline (PBS) followed by 4% paraformaldehyde (PFA) in PBS. For embryonic tissue collection, pregnant dams were deeply anesthetized with isoflurane, euthanized by cervical dislocation, and embryos were immediately harvested by cesarean section. All efforts were made to minimize animal pain, discomfort, and distress throughout the procedures.

Tissue preparation and immunohistochemical staining

The animals underwent immunohistochemistry staining to quantify the number of interneurons expressing somatostatin.

Embryonic mice (E14.5, E15.5 and E16.5) were dissected, and their brains were embedded in 4% agarose. Coronal sections, 50 µm-thick, were then cut using a vibratome (Leica VT1000S). These sections, which were free-floating, underwent RFP immunohistochemistry. First, the tissue was rinsed with phosphate buffer solution containing 0.075% Triton X-100 (PBS-T) and processed for immunohistochemistry staining. Subsequently, the tissue was incubated with 10% Goat serum (GS) (blocking solution) for 1 h to prevent any nonspecific antigen binding. Next, the sections were incubated overnight at 4 °C with the proper primary antibody diluted in EnVision FLEX Antibody Diluent (DAKO, Denmark). The antibodies used were rabbit anti-RFP polyclonal (1:500, ab62341/ABCAM). On the following day, the sections were rinsed three times at room temperature and then incubated with the secondary antibody for 1 h: anti-rabbit IgG conjugated with Cy3-streptavidin (1:500, BA-1000//Vector; PA43001//Amersham) for rabbit anti-RFP polyclonal. After this incubation, the sections were washed with PBS-T.

To delineate anatomical regions such as the MZ, CP and SVZ sections were counterstained with 4',6-diamidino-2-phenylindole (DAPI; *Molecular Probes/Invitrogen*, 1:10.000 in PBS) for 10 min. Finally, the sections were mounted on glass slides using a mounting medium composed of 10:1 Mowiol (Calbiochem) and NPG (Sigma).

For postnatal mice at P1, brains were dissected and embedded in 4% agarose. Coronal sections, each 50 µm thick, were then cut using a vibratome. These sections, which were free-floating, underwent overnight incubation with the primary antibody, rabbit anti-SST IgG (1:300, *Invitrogen*, PA5-85759) or rabbit anti-Caspase-3 (1:200, *Abcam*, ab2302) diluted in DAKO. The following day, the sections were rinsed three times and incubated with the secondary antibody for 1 h with the secondary antibody: donkey Alexa Fluor 488 anti-rabbit IgG (1:500, A 21206//Invitrogen) for rabbit anti-SST or biotinylated goat anti-rabbit IgG (1:200, *Vector Laboratories*, BA1000) for rabbit anti-Caspase-3. For SST detection, following incubation, the sections were washed with PBS-T and counterstained with DAPI for 10 min. Finally, the sections were mounted on glass slides using a mounting medium composed of Mowiol (Calbiochem) and NPG (Sigma) in a 10:1 ratio. For Caspase-3 detection, after washing the primary antibody, the sections were incubated with the Avidin-Biotin Complex (ABC) for 1 h at a dilution of 1:300 (ABC Kit, *Vector Laboratories*, CA-94010). For brown colorimetric detection, the tissue was incubated in a solution containing 1% 3,3′-Diaminobenzidine (DAB; *Vector Laboratories*, SK-4100) and 0.0018% hydrogen peroxide (H_2O_2) in PBS. Subsequently, the sections were washed with PBS, dehydrated and mounted using Eukitt (O. Kindler GmbH & Co., Freiburg).

For postnatal mice (P30), the brains were progressively dehydrated in ethanol, embedded in paraffin and then sliced into 16 µm-thick coronal sections using microtome (Leica). These sections were mounted in four parallel series. The first series of sections underwent dewaxing and rehydration, followed by processing for somatostatin immunohistochemistry staining. Initially, the sections were immersed in 0,9% hydrogen peroxide (H_2O_2) for 30 min to block endogenous peroxidase activity, and then rinsed with PBS-T. Subsequently, the tissue was incubated with goat serum (GS) for 1 h. The sections were incubated overnight with the primary antibody, rabbit anti-SST IgG (1:300, *Invitrogen*, PA5-85759) diluted in DAKO. The following day, the sections were rinsed three times and incubated with the biotinylated secondary antibody (1:200; Vector BA-1000) for 1 h. After washing with PBS-T, the sections were incubated with Avidin-Biotin Complex for 1 h (1:300; ABC kit Vector Laboratories CA-94010). For colorimetric detection (black), the tissue was incubated with 1% 3,39-Diaminobenzidine (DAB; Vector Laboratories SK-4100), 0.025% ammonium nickel sulfate hexahydrate, and 0.0018% H_2O_2 in PBS. Next, the sections were washed with PBS and stained with cresyl violet to identify the anatomical boundaries of cortical layers (II-VI). Finally, the sections were dehydrated and mounted in Eukitt (O.Kindler GmbH and CO, Freiburg).

Microscopy, stereological quantification and statistical analysis

SST+ cells in ACA and RSC at P30 of each hemisphere were quantified using a Leica DM4000 microscope coupled to stereological software (StereoInvestigator, MBF Bioscience, Williston, VT, USA) employing the Optical Fractionator probe. Initially, the layers II/III, V, and VI of ACA and RSC were outlined at low magnifications using a 2,5x objective lens. The number of sections to be analyzed, their interval and the thickness were determined (7 sections, 16 µm and regular interval 24 sections – 384 µm-).

Subsequently, SST+ interneurons within the 3-dimensional optical dissector were counted at a higher magnification using a 63x objective lens. Square grids were systematically and randomly placed over the layers of ACA and RSC. For neuronal counting, a counting frame (100 × 100) within the optical dissector was utilized. The height (thickness) of the optical dissector was set at 9 µm with a top guard zone of 3,5 µm. SST+ interneurons were easily distinguished by focusing up and down, and only SST+ cell bodies within the optical dissector height were counted. The precision of the quantification was assessed based on the Gundersen error coefficient, m = 1 (CE). For optimal estimation, the Gundersen error coefficient (CE) with m = 1 should ideally be less than or equal to 0.1.

Cells expressing Caspase-3 in basal telencephalon were quantified following a similar procedure. Initially, the region of interest was outlined at low magnifications using a 2,5x objective lens. The number of sections to be analyzed, their interval and the thickness were determined (7 sections, 50 µm and regular interval 2 sections – 100 µm-).

For analysis of development, images were acquired using confocal microscopes (Leica TCS SPE). Images stained with RFP immunohistochemistry were quantified using Image J software (NIH, United States). Anatomical regions (MZ, CP, SP, IZ and SVZ) were determined using DAPI counterstaining. To quantify the number of SST+ cells, six hemispheres were used. For each hemisphere, four images spanning rostral to caudal regions of the cortex were captured and treated as technical replicates.

The morphological analysis of migrating cells was performed using a Leica DM4000 microscope coupled to the Neurolucida software (MBF Bioscience, Williston, VT, USA). To enhance the RFP fluorescent signal in interneurons selected for morphological assessment, immunohistochemistry against RFP was carried out on 50 µm-thick coronal sections prepared with a Leica VT1000S vibratome at embryonic stage E15.5. Interneurons migrating tangentially through the intermediate zone were selected for morphological analysis once they reached the dorsal pallium. The analyzed region was defined by a rectangle with a short side measuring 150 µm, whose center was positioned near the ventricular apex. Individual cells were manually traced to reconstruct their morphology and migratory trajectories. From these tracings, morphological parameters such as soma perimeter and elongation index were quantified. Morphological analysis was performed using six hemispheres. For each hemisphere, six coronal Sect. (50 µm thick) were selected and a total of 30 to 36 SST-RFP–expressing interneurons were randomly selected along the intermediate zone of the tangential migratory stream for detailed morphological assessment.

The SST-RFP positives were assessed with the area fraction fractionator (AFF) probe. The probe is designed to estimate the fraction of a region occupied by a sub-region (SST-RFP). This area fraction probe is implemented by performing a fractionator scan of the area of interest (basal forebrain) while overlaying a grid of points. Initially, the areas of interest were outlined at low magnifications using a 2,5x objective lens. The number of sections to be analyzed, their interval and the thickness were determined (5 sections, 50 µm, regular interval 6 sections – 300 µm-). Subsequently, SST-RFP positive within AFF were analyzed at a higher magnification using a 20x objective lens. A counting frame (100 × 100) was utilized. We mark the points for the sub-region, the SST-RFP signal, and the points for the region of interest, that is the ventral region of the forebrain. The precision of the quantification was assessed based on the Gundersen error coefficient, m = 1 (CE). For optimal estimation, the Gundersen error coefficient (CE) with m = 1 should ideally be less than or equal to 0.1.

Since the data from some experimental groups of P30 and from morphological analysis did not fulfill the criteria for the use of parametric statistical tests, we decided to use only non-parametrical tests for all statistical comparisons. We used the Mann-Whitney test (rank sum test) for the comparison between the data from mutant animals with controls. For the comparison of the number or density of cells among cortical layers we used the Kruskal-Wallis (ANOVA on ranks) test, with post-hoc Tukey or Dunn test used for pairwise comparison (data groups with same or different number of cases respectively). All data are given as mean ± standard deviation, with indication of the number of cases.

For the experimental group of E14.5, E15.5, E16.5 and P1, which fulfill the criteria for the use of parametric statistical tests, we used Student's t-test. Statistical significance was considered at a p-value of less than 0.05, denoted as $*p<0.05$, $**p<0.01$ and $***p<0.001$.

Data availability

Data is provided within the manuscript.

Received: 30 July 2025; Accepted: 29 January 2026
Published online: 04 February 2026

References

1. Reiner, O. et al. Isolation of a Miller-Dieker lissencephaly gene containing G protein beta-subunit-like repeats. *Nature* **364**, 717–721 (1993).
2. Reiner, O. LIS1. Let's interact sometimes… part 1). *Neuron* **28**, 633–636 (2000).
3. Hirotsune, S. et al. Graded reduction of Pafah1b1 (Lis1) activity results in neuronal migration defects and early embryonic lethality. *Nat. Genet.* **19**, 333–339 (1998).

4. Paylor, R. et al. Impaired learning and motor behavior in heterozygous Pafah1b1 (Lis1) mutant mice. *Learn. Mem.* **6**, 521–537 (1999).
5. Fleck, M. W. et al. Hippocampal abnormalities and enhanced excitability in a murine model of human lissencephaly. *J. Neurosci.* **20**, 2439–2450 (2000).
6. Dinday, M. T., Girskis, K. M., Lee, S., Baraban, S. C. & Hunt, R. F. PAFAH1B1 haploinsufficiency disrupts GABA neurons and synaptic E/I balance in the dentate gyrus. *Sci. Rep.* **7**, 8269 (2017).
7. Hunt, R. F., Dinday, M. T., Hindle-Katel, W. & Baraban, S. C. LIS1 deficiency promotes dysfunctional synaptic integration of granule cells generated in the developing and adult dentate gyrus. *J. Neurosci.* **32**, 12862–12875 (2012).
8. Jones, D. L. & Baraban, S. C. Inhibitory inputs to hippocampal interneurons are reorganized in Lis1 mutant mice. *J. Neurophysiol.* **102**, 648–658 (2009).
9. Cahana, A. et al. Targeted mutagenesis of Lis1 disrupts cortical development and LIS1 homodimerization. *Proc. Natl. Acad. Sci. U S A*. **98**, 6429–6434 (2001).
10. Reiner, O., Cahana, A., Escamez, T. & Martinez, S. LIS1-no more no less. *Mol. Psychiatry*. **7**, 12–16 (2002).
11. Garcia-Lopez, R., Pombero, A., Dominguez, E., Geijo-Barrientos, E. & Martinez, S. Developmental alterations of the septohippocampal cholinergic projection in a lissencephalic mouse model. *Exp. Neurol.* **271**, 215–227 (2015).
12. Garcia-Lopez, R., Pombero, A., Estirado, A., Geijo-Barrientos, E. & Martinez, S. Interneuron heterotopia in the Lis1 mutant mouse cortex underlies a structural and functional Schizophrenia-Like phenotype. *Front. Cell. Dev. Biol.* **9**, 693919 (2021).
13. Wonders, C. P. & Anderson, S. A. The origin and specification of cortical interneurons. *Nat. Rev. Neurosci.* **7**, 687–696 (2006).
14. Marín, O. & Rubenstein, J. L. A long, remarkable journey: tangential migration in the telencephalon. *Nat. Rev. Neurosci.* **2**, 780–790 (2001).
15. Butt, S. J. B. et al. The Temporal and Spatial origins of cortical interneurons predict their physiological subtype. *Neuron* **48**, 591–604 (2005).
16. Miyoshi, G., Butt, S. J. B., Takebayashi, H. & Fishell, G. Physiologically distinct Temporal cohorts of cortical interneurons arise from telencephalic Olig2-expressing precursors. *J. Neurosci.* **27**, 7786–7798 (2007).
17. Xu, Q., Cobos, I., De La Cruz, E., Rubenstein, J. L. & Anderson, S. A. Origins of cortical interneuron subtypes. *J. Neurosci.* **24**, 2612–2622 (2004).
18. Lim, L. et al. Optimization of interneuron function by direct coupling of cell migration and axonal targeting. *Nat. Neurosci.* **21**, 920–931 (2018).
19. Tanaka, D. H. et al. Random walk behavior of migrating cortical interneurons in the marginal zone: time-lapse analysis in flat-mount cortex. *J. Neurosci.* **29**, 1300–1311 (2009).
20. Pla, R., Borrell, V., Flames, N. & Marín, O. Layer acquisition by cortical GABAergic interneurons is independent of reelin signaling. *J. Neurosci.* **26**, 6924–6934 (2006).
21. Lim, L., Mi, D., Llorca, A. & Marín, O. Development and functional diversification of cortical interneurons. *Neuron* **100**, 294–313 (2018).
22. Southwell, D. G. et al. Intrinsically determined cell death of developing cortical interneurons. *Nature* **491**, 109–113 (2012).
23. Miyoshi, G. et al. Genetic fate mapping reveals that the caudal ganglionic eminence produces a large and diverse population of superficial cortical interneurons. *J. Neurosci.* **30**, 1582–1594 (2010).
24. Xu, X., Roby, K. D. & Callaway, E. M. Immunochemical characterization of inhibitory mouse cortical neurons: three chemically distinct classes of inhibitory cells. *J. Comp. Neurol.* **518**, 389–404 (2010).
25. Rudy, B., Fishell, G., Lee, S. & Hjerling-Leffler, J. Three groups of interneurons account for nearly 100% of neocortical GABAergic neurons. *Dev. Neurobiol.* **71**, 45–61 (2011).
26. Baraban, S. C. & Tallent, M. K. Interneuron diversity series: interneuronal neuropeptides–endogenous regulators of neuronal excitability. *Trends Neurosci.* **27**, 135–142 (2004).
27. Grilli, M., Raiteri, L. & Pittaluga, A. Somatostatin inhibits glutamate release from mouse cerebrocortical nerve endings through presynaptic sst2 receptors linked to the adenylyl cyclase-protein kinase A pathway. *Neuropharmacology* **46**, 388–396 (2004).
28. Martel, G., Dutar, P., Epelbaum, J. & Viollet, C. Somatostatinergic systems: an update on brain functions in normal and pathological aging. *Front. Endocrinol.* **3**, 154 (2012).
29. Benes, F. M., McSparren, J., Bird, E. D., SanGiovanni, J. P. & Vincent, S. L. Deficits in small interneurons in prefrontal and cingulate cortices of schizophrenic and schizoaffective patients. *Arch. Gen. Psychiatry*. **48**, 996–1001 (1991).
30. Tripp, A., Kota, R. S., Lewis, D. A. & Sibille, E. Reduced somatostatin in subgenual anterior cingulate cortex in major depression. *Neurobiol. Dis.* **42**, 116–124 (2011).
31. Seney, M. L., Tripp, A., McCune, S., Lewis, D. A. & Sibille, E. Laminar and cellular analyses of reduced somatostatin gene expression in the subgenual anterior cingulate cortex in major depression. *Neurobiol. Dis.* **73**, 213–219 (2015).
32. Vogt, B. *Cingulate Neurobiology and Disease* (Oxford University Press, 2009).
33. van Heukelum, S. et al. Where is cingulate cortex? A Cross-Species view. *Trends Neurosci.* **43**, 285–299 (2020).
34. Vogt, B. A. & Peters, A. Form and distribution of neurons in rat cingulate cortex: areas 32, 24, and 29. *J. Comp. Neurol.* **195**, 603–625 (1981).
35. Vogt, B. A. & Paxinos, G. Cytoarchitecture of mouse and rat cingulate cortex with human homologies. *Brain Struct. Funct.* **219**, 185–192 (2014).
36. Kocher, M. et al. Individual variability in the anatomical distribution of nodes participating in rich club structural networks. *Front. Neural Circuits*. **9**, 16 (2015).
37. Rolls, E. T. The cingulate cortex and limbic systems for emotion, action, and memory. *Brain Struct. Funct.* **224**, 3001–3018 (2019).
38. Vann, S. D., Aggleton, J. P. & Maguire, E. A. What does the retrosplenial cortex do? *Nat. Rev. Neurosci.* **10**, 792–802 (2009).
39. Akbarian, S., Smith, M. A. & Jones, E. G. Editing for an AMPA receptor subunit RNA in prefrontal cortex and striatum in alzheimer's disease, huntington's disease and schizophrenia. *Brain Res.* **699**, 297–304 (1995).
40. Sibille, E., Morris, H. M., Kota, R. S. & Lewis, D. A. GABA-related transcripts in the dorsolateral prefrontal cortex in mood disorders. *Int. J. Neuropsychopharmacol.* **14**, 721–734 (2011).
41. Batista-Brito, R., Machold, R., Klein, C. & Fishell, G. Gene expression in cortical interneuron precursors is prescient of their mature function. *Cereb. Cortex*. **18**, 2306–2317 (2008).
42. Petros, T. J., Bultje, R. S., Ross, M. E., Fishell, G. & Anderson, S. A. Apical versus basal neurogenesis directs cortical interneuron subclass fate. *Cell. Rep.* **13**, 1090–1095 (2015).
43. Puelles, L. et al. Radial and tangential migration of telencephalic somatostatin neurons originated from the mouse diagonal area. *Brain Struct. Funct.* **221**, 3027–3065 (2016).
44. Munguba, H. et al. Transcriptional maintenance of cortical somatostatin interneuron subtype identity during migration. *Neuron* **111**, 3590–3603e5 (2023).
45. Inan, M., Welagen, J. & Anderson, S. A. Spatial and Temporal bias in the mitotic origins of somatostatin- and parvalbumin-expressing interneuron subgroups and the chandelier subtype in the medial ganglionic eminence. *Cereb. Cortex*. **22**, 820–827 (2012).
46. Scholzen, T. & Gerdes, J. The Ki-67 protein: from the known and the unknown. *J. Cell. Physiol.* **182**, 311–322 (2000).
47. Anderson, S. A., Eisenstat, D. D., Shi, L. & Rubenstein, J. L. Interneuron migration from basal forebrain to neocortex: dependence on Dlx genes. *Science* **278**, 474–476 (1997).

48. Hu, J. S., Vogt, D., Sandberg, M. & Rubenstein, J. L. Cortical interneuron development: a Tale of time and space. *Development* **144**, 3867–3878 (2017).
49. Riedemann, T. Diversity and function of Somatostatin-Expressing interneurons in the cerebral cortex. *Int J. Mol. Sci* **20**, 2952 (2019).
50. Sudarov, A., Gooden, F., Tseng, D., Gan, W. B. & Ross, M. E. Lis1 controls dynamics of neuronal filopodia and spines to impact synaptogenesis and social behaviour. *EMBO Mol. Med.* **5**, 591–607 (2013).
51. Reiner, O., Sapoznik, S. & Sapir, T. Lissencephaly 1 linking to multiple diseases: mental retardation, neurodegeneration, schizophrenia, male sterility, and more. *Neuromolecular Med.* **8**, 547–565 (2006).
52. Tabarés-Seisdedos, R. et al. Evidence for association between structural variants in lissencephaly-related genes and executive deficits in schizophrenia or bipolar patients from a Spanish isolate population. *Psychiatr Genet.* **18**, 313–317 (2008).
53. Domínguez-Sala, E. et al. Abnormalities in cortical GABAergic interneurons of the primary motor cortex caused by mutation produce a Non-drastic functional phenotype. *Front. Cell. Dev. Biol.* **10**, 769853 (2022).
54. Jones, D. L. & Baraban, S. C. Characterization of inhibitory circuits in the malformed hippocampus of Lis1 mutant mice. *J. Neurophysiol.* **98**, 2737–2746 (2007).
55. Kato, M. A new paradigm for West syndrome based on molecular and cell biology. *Epilepsy Res.* **70** (Suppl 1), S87–95 (2006).
56. Cahana, A., Jin, X. L., Reiner, O., Wynshaw-Boris, A. & O'Neill, C. A study of the nature of embryonic lethality in LIS1-/- mice. *Mol. Reprod. Dev.* **66**, 134–142 (2003).
57. Valdés-Sánchez, L. et al. Postnatal alterations of the inhibitory synaptic responses recorded from cortical pyramidal neurons in the Lis1/sLis1 mutant mouse. *Mol. Cell. Neurosci.* **35**, 220–229 (2007).
58. Domínguez-Sala, E. et al. Properties of the epileptiform activity in the cingulate cortex of a mouse model of LIS1 dysfunction. *Brain Struct. Funct.* **227**, 1599–1614 (2022).
59. Song, Y. H., Yoon, J. & Lee, S. H. The role of neuropeptide somatostatin in the brain and its application in treating neurological disorders. *Exp. Mol. Med.* **53**, 328–338 (2021).
60. Davies, P., Katzman, R. & Terry, R. D. Reduced somatostatin-like immunoreactivity in cerebral cortex from cases of alzheimer disease and alzheimer senile Dementa. *Nature* **288**, 279–280 (1980).
61. Terry, R. D. & Katzman, R. Senile dementia of the alzheimer type. *Ann. Neurol.* **14**, 497–506 (1983).
62. Iwasawa, C. et al. Reduced expression of somatostatin in GABAergic interneurons derived from induced pluripotent stem cells of patients with parkin mutations. *Mol. Brain*. **12**, 5 (2019).
63. Holley, S. M., Galvan, L., Kamdjou, T., Cepeda, C. & Levine, M. S. Striatal GABAergic interneuron dysfunction in the Q175 mouse model of huntington's disease. *Eur. J. Neurosci.* **49**, 79–93 (2019).
64. Konradi, C. et al. Hippocampal interneurons are abnormal in schizophrenia. *Schizophr Res.* **131**, 165–173 (2011).
65. Lipska, B. K. et al. Expression of DISC1 binding partners is reduced in schizophrenia and associated with DISC1 SNPs. *Hum. Mol. Genet.* **15**, 1245–1258 (2006).
66. Bradshaw, N. J. et al. PKA phosphorylation of NDE1 is DISC1/PDE4 dependent and modulates its interaction with LIS1 and NDEL1. *J. Neurosci.* **31**, 9043–9054 (2011).
67. Matsumoto, N. et al. Mutation analysis of the DCX gene and genotype/phenotype correlation in subcortical band heterotopia. *Eur. J. Hum. Genet.* **9**, 5–12 (2001).
68. Reiner, O. & Sapir, T. LIS1 functions in normal development and disease. *Curr. Opin. Neurobiol.* **23**, 951–956 (2013).
69. Toudji, I., Toumi, A., Chamberland, É. & Rossignol, E. Interneuron odyssey: molecular mechanisms of tangential migration. *Front. Neural Circuits*. **17**, 1256455 (2023).
70. Reiner, O. LIS1 and DCX: implications for brain development and human disease in relation to microtubules. *Scientifica* **2013**, 393975 (2013).
71. Shu, T. et al. Ndel1 operates in a common pathway with LIS1 and cytoplasmic dynein to regulate cortical neuronal positioning. *Neuron* **44**, 263–277 (2004).
72. McManus, M. F., Nasrallah, I. M., Pancoast, M. M., Wynshaw-Boris, A. & Golden, J. A. Lis1 is necessary for normal non-radial migration of inhibitory interneurons. *Am. J. Pathol.* **165**, 775–784 (2004).
73. Nasrallah, I. M., McManus, M. F., Pancoast, M. M., Wynshaw-Boris, A. & Golden, J. A. Analysis of non-radial interneuron migration dynamics and its disruption in Lis1+/- mice. *J. Comp. Neurol.* **496**, 847–858 (2006).
74. Gopal, P. P., Simonet, J. C., Shapiro, W. & Golden, J. A. Leading process branch instability in Lis1+/- nonradially migrating interneurons. *Cereb. Cortex*. **20**, 1497–1505 (2010).
75. Youn, Y. H., Pramparo, T., Hirotsune, S. & Wynshaw-Boris, A. Distinct dose-dependent cortical neuronal migration and neurite extension defects in Lis1 and Ndel1 mutant mice. *J. Neurosci.* **29**, 15520–15530 (2009).
76. Gambello, M. J. et al. Multiple dose-dependent effects of Lis1 on cerebral cortical development. *J. Neurosci.* **23**, 1719–1729 (2003).
77. Su, P. et al. Disruption of SynGAP-dopamine D1 receptor complexes alters actin and microtubule dynamics and impairs GABAergic interneuron migration. *Sci Signal* **12**, eaau9122 (2019).
78. Tivodar, S. et al. Rac-GTPases regulate microtubule stability and axon growth of cortical GABAergic interneurons. *Cereb. Cortex*. **25**, 2370–2382 (2015).
79. Lee, K., Ireland, K., Bleeze, M. & Shoubridge, C. ARX polyalanine expansion mutations lead to migration impediment in the rostral cortex coupled with a developmental deficit of calbindin-positive cortical GABAergic interneurons. *Neuroscience* **357**, 220–231 (2017).

Acknowledgements

We would like to thank M. Garcia and F. Almagro for their excellent technical assistance.

Author contributions

Ana Pombero: Conceptualization, formal analysis, investigation, writing-original draft ; Raquel Garcia-Lopez: Conceptualization, formal analysis, investigation, writing-original draft; Emilio Geijo-Barrientos: Conceptualization, supervision, writing-review and editing; Salvador Martinez: Conceptualization, supervision, writing-review and editing.

Funding

Declaration. This work was supported by the Spanish State Research Agency, through the "Severo Ochoa" Programme for Centres of Excellence in R&D (Grant Numbers SEV-2017-0723), the Spanish Ministerio de Ciencia e Innovación grant numbers SAF2017-83702-R and PID2020-11817RB-I00 and the Generalitat Valenciana (program Prometeo II, Grant Number 2018/041).

Declarations

Competing interests
The authors declare no competing interests.

Additional information
Correspondence and requests for materials should be addressed to R.G.-L. or S.M.

Reprints and permissions information is available at www.nature.com/reprints.

Publisher's note Springer Nature remains neutral with regard to jurisdictional claims in published maps and institutional affiliations.